Crystal Structure of Alternating Isotactic Ethylene−Cyclopentene Copolymer

Finizia Auriemma,* Claudio De Rosa, and Simona Esposito

Dipartimento di Chimica, Università di Napoli "Federico II", Complesso Monte S. Angelo, Via Cintia, 80126 Napoli, Italy

Geoffrey W. Coates and Masayuki Fujita

Department of Chemistry and Chemical Biology, Baker Laboratory, Cornell University, Ithaca, New York 14853-1301

Received March 30, 2005; Revised Manuscript Received June 9, 2005

ABSTRACT: The crystal structure of an alternating isotactic ethylene (E)−cyclopentene (C) copolymer (ECC) has been studied on the basis of X-ray diffraction, geometrical, and conformational analyses of the single chain and packing energy calculations. A value of chain axis periodicity of 9.0 Å has been evaluated from X-ray diffraction patterns. Geometrical and conformational energy calculations have shown that isotactic ECC chains assume nearly extended conformations in the crystalline state, having **t***i* or **s**(2/1)*m* symmetry according to the experimental chain axis periodicity. A high degree of conformational disorder is present in the crystalline state related to the conformational freedom of the cyclopentene rings which may assume twist (C_2-symmetric) and envelope (C_s-symmetric) conformations interconverting with a low-energy barrier. The conformation of the chains in the crystalline state is of kind $(T_3\ \theta\ T_3\ -\theta)_n$ with θ variable in the range −50° to +50°, depending on the conformation of the five-membered rings, and corresponds to the repetition of anticlined enantiomorphic structural units along the chain. ECC represents a rare example of an isotactic polymer which assumes in the crystalline state a conformation that does not correspond to a helical repetition of isoclinic, isomorphous structural units. Depending on the succession of configurations $(RS)_n$ or $(SR)_n$ of tertiary carbon atoms in consecutive cyclopentene rings, the polymer chains may assume Z- or S-shapes. Chains in **t***i* or **s**(2/1)*m* conformation are packed in an orthorhombic unit cell with axes $a = 7.83$ Å, $b = 8.76$ Å, and $c = 9.0$ Å. Dynamic conformational disorder and packing disorder due to the statistical substitution of chains having S- and Z-shapes are present. The structure may be described by statistical space groups *Pcan* and/or *Ccmm* for **t***i* and **s**(2/1)*m* conformations, respectively.

Introduction

Development of single-center homogeneous catalytic systems has allowed the homo- and copolymerization of strained cyclic olefins as cyclopentene, norbornene, and their substituted compounds.[1] Polymerization of cycloolefins using *ansa*-zirconocene complexes,[1,2] or other homogeneous catalysts, occurs via exclusive *cis*-addition to the double bond.[1−3] Use of chiral metallocenes may yield tactic, crystalline, practically insoluble homopolymers, with extremely high melting point, up to 400 °C, and high chemical resistance; in most cases decomposition occurs before melting.[1,4] Because of their high melting points, tactic polycyclolefins are not easily processable. On the other hand, atactic homopolymers may be produced by nonchiral metallocenes such as Cp_2ZrCl_2 (Cp = cyclopentadienyl); these materials are amorphous glasses, present high glass transition temperature, and can be dissolved in hydrocarbon solvents.[1,4]

Use of homogeneous catalytic systems allows also copolymerization of cyclic olefins with ethylene or α-olefins.[1] Cyclic olefins copolymers (COCs) represent a class of thermoplastic materials of growing interest, with mechanical and physical properties ranging from those of amorphous glasses to those of thermoplastic elastomers.[5−8]

Early attempts to produce alternating copolymers of ethylene and olefins with both the carbon atoms of the double bond carrying substituent organic groups (as for instance 2-butene) were made by Natta et al.[9] using anionic coordination Ziegler−Natta catalysts. Natta recognized that alternating copolymers were accessible due to the reticence of many coordination catalysts to homopolymerize olefins with internal double bond. In particular, the synthesis of ethylene/*cis*-butene-2[9a] and ethylene/cyclopentene[9b] alternating copolymers was achieved in the early 1960s using vanadium compounds as precatalysts and alkylaluminum as cocatalyst and a low ethylene pressure. By fractionation procedures of crude products in boiling solvents, highly crystalline fractions were obtained with characteristic X-ray diffraction patterns, well different from that of crystalline polyethylene.[9] The crystallinity of these copolymers was taken as indicative of the regularity of the chemical and steric structure.[10] At that time it was not possible to establish the steric microstructure of the macromolecular chains by NMR. Although it was recognized that the catalytic species act through a *cis*-addition to the double bond,[9] the attribution of a *meso*-diisotactic microstructure was based merely upon X-ray diffraction analysis.[10]

Later, Kaminsky et al. described the copolymerization of ethylene with cyclopentene, norbornene, and other cycloolefins, with homogeneous zirconocene catalysts.[1,4] It was shown that through the rational choice of the metallocene catalyst precursor the microstructure of ethylene/cycloolefins copolymers may be varied from statistical to alternating and from atactic to fully stereoregular, obtaining materials with unprecedented microstructures and properties. The physical properties

* To whom correspondence should be addressed: Tel ++39 081 674341; Fax ++39 081 674090; e-mail finizia.auriemma@unina.it.

10.1021/ma050659v CCC: $30.25
Published on Web 07/27/2005

of these copolymers, indeed, depend not only on the type of cycloolefin but also on the composition and sequence distribution of comonomeric units and the degree of stereoregularity. For instance, random ethylene−cycloolefins copolymers are amorphous glasses with a wide range of glass-transition temperatures, good thermal stability, and chemical resistance;[1,4] alternating ethylene−norbornene copolymers, instead, are crystalline materials, independent of the kind and degree of stereoregularity, with good transparency and high melting temperatures (295 °C for the isotactic copolymer).[1,4,8,11−15] It is worth noting that, while the ethylene−cyclopentene copolymers produced with vanadium-based catalysts show exclusive 1,2-enchainment of cyclopentene rings, those obtained with zirconocene catalysts have a mixed microstructure of 1,2- and 1,3-enchained cyclopentene units.[1,16−20]

Recently, alternating and multiblock ethylene−cyclopentene copolymers have been obtained using a living bis(phenoxyimine)titanium catalyst.[21] They are atactic and characterized by narrow distribution of molecular weights and exclusive 1,2-enchainment of cyclopentene rings along the chain. The alternating copolymers are amorphous materials, with glass transition temperatures increasing linearly with increasing cyclopentene content from −30 to 10 °C. In addition, ring-opening metathesis polymerization (ROMP) of bicyclo[3.2.0]hept-6-ene was also employed to obtain ethylene−cyclopentene copolymers with a strictly alternating structure and high molecular weight. More precisely, the metathesis polymerization of bicyclo[3.2.0]hept-6-ene was performed using, in a case, an achiral ruthenium carbene complex and poly(bicyclo[3.2.0]hept-6-ene), including in the main chain double bonds in the *cis*- and *trans*-configuration, was obtained.[21] In a second case, a chiral molybdenum carbene complex was used, and a highly *cis*-tactic poly(bicyclo[3.2.0]hept-6-ene) was obtained.[21] The unsaturated polymers were successively hydrogenated to give in the first case a poorly stereoregular, slightly syndiotactic ethylene−cyclopentene copolymer (ECC), melting at 123 °C, and in the second case a highly isotactic ECC, melting at 182 °C,[21] close to the melting temperature of early ECC products (185 °C).[9]

The alternating stereospecific copolymerization of ethylene with cyclopentene has also been achieved using a new class of constrained geometry titanium catalysts.[22,23] Depending on the kind of ligand, alternating atactic or stereoregular ECCs were obtained. In particular, use of chiral constrained geometry Ti complexes allowed obtaining alternating ECCs with isotactic *cis*-1,2-cyclopentene enchainment. These copolymers are crystalline, with melting temperature of 183 °C,[22] analogous to the octane-insoluble fractions of ECCs obtained using vanadium-based catalyst systems[9b] and the isotactic ECC obtained by the ROMP mechanism.[21]

Although alternating diisotactic copolymers of ethylene and olefins with internal double bonds as butene-2 and cyclopentene were obtained already in the 1960s,[9] the complete determination of the crystal structure was reported only in the case of the alternating *meso*-diisotactic ethylene/*cis*-butene-2 copolymer.[10c] Only preliminary data concerning the chain conformation in the crystalline state and the dimensions of the unit cell have been reported at that time in the case *meso*-diisotactic ECC.[10a,b]

In light of the refocused interest for ECCs as a novel class of engineering plastics, we have investigated the crystal structure of alternating *meso*-diisotactic ECC. A preliminary model of crystal structure of ECC has been recently published, showing that a high degree of structural disorder is included in the crystals, related to the conformational freedom of cyclopentene rings, and to statistical substitution of ECC chains with different shape in the lattice positions.[24]

Scheme 1. Synthesis of Isotactic Poly(*cis*-cyclopentene-*alt*-ethylene)

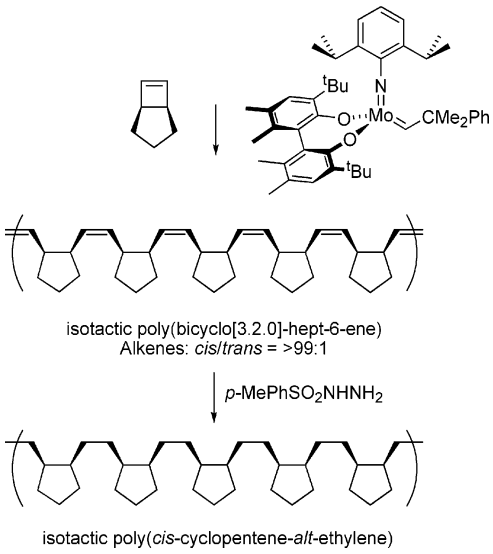

In this paper the crystal structure and the corresponding structural disorder of ECC are described in detail. A careful analysis of X-ray diffraction patterns of unoriented and oriented ECC samples is performed along with a detailed analysis of structural disorder by conformational and packing energy calculations.

Experimental Part and Methods of Calculation

A strictly alternating, *meso*-diisotactic ethylene−cyclopentene copolymer (ECC) sample was obtained by ring-opening metathesis polymerization (ROMP) of bicyclo[3.2.0]hept-6-ene using a chiral molybdenum−carbene complex[25] and successive hydrogenation of unsaturated copolymer, following, with small differences, the procedure described in ref 21 (see Scheme 1). The method and conditions of preparation of ECC sample are described in the Supporting Information. The average molecular weight (M_n) and the molecular weight distribution (M_w/M_n) determined by GPC analysis in 1,2,4-trichlorobenzene at 140 °C vs polystyrene standard are 41 900 g/mol and 2.07, respectively.

The alternating ECC sample presents, as prepared, two melting peaks at 179 and 191 °C due to melting and recrystallization phenomena, whereas the crystallization temperature occurs at 156 °C (determined with a differential scanning calorimeter Perkin-Elmer DSC 7, flowing N_2 atmosphere, scanning rate 10 °C/min). ^{13}C NMR analysis indicates a high degree of tacticity due to a *meso*-diisotactic microstructure.

Unoriented films used for structural analysis have been obtained by compression molding of as-polymerized samples. The powders samples have been heated at 215 °C between perfectly flat brass plates under a press at very low pressure, kept at 215 °C for 10 min, and quenched in N_2(l). Crystalline oriented fibers were obtained by stretching strips cut from compression-molded films (3 mm width, 0.8 mm thick, 20 mm long) at 160 °C up to 3.6 times the initial length and successive annealing at 150 °C for 30 min.

X-ray powder diffraction patterns were obtained with an automatic Philips diffractometer (Ni-filtered Cu Kα radiation). The X-ray fiber diffraction patterns were recorded on a BAS-MS imaging plate (FUJIFILM) using a cylindrical camera and

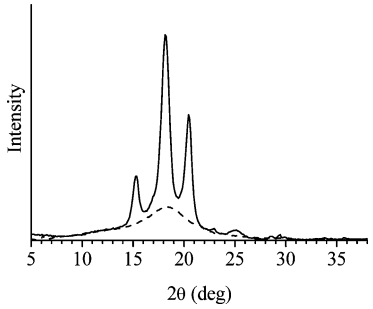

Figure 1. X-ray powder diffraction profile of as-prepared ECC sample (solid line) and of the amorphous phase (dashed line) after subtraction of a straight baseline approximating the background.

processed with a digital imaging reader (FUJIBAS 1800) (Cu $K\alpha_1$ radiation, monochromatized with a graphite single crystal).

Calculated structure factors were obtained as $F_c = (\sum|F_i|^2M_i)^{1/2}$, where F_i is the structure factor and M_i the multiplicity factor of the reflection i (Miller indices $(h\ k\ l)_i$) in powder diffraction patterns, and the summation is taken over all reflections included in the 2θ range of the corresponding diffraction peak observed in the X-ray powder diffraction profile. A thermal factor $B = 12$ Å^2 and atomic scattering factors as in ref 26 were assumed.

The observed structure factors, F_o, were evaluated from the intensities of the reflections observed in the powder diffraction profiles, $F_o = (I_o/LP)^{1/2}$, where LP is the Lorentz-polarization factor for X-ray powder diffraction.[27a] The experimental intensities I_o were evaluated by measuring the area of the peaks in the X-ray powder diffraction profile, after subtraction of a straight baseline approximating the background and of the amorphous halo. For the amorphous profile the diffraction pattern of the melted sample has been used. The position of the maximum in the amorphous pattern has been obtained by extrapolating to room temperature the 2θ positions of the maxima in diffraction profiles of melt recorded at different temperatures.

The intensity of Bragg reflections in the X-ray fiber diffraction patterns were qualitatively compared with calculated intensities I_c. The calculated intensities values have been obtained as $I_c = |F_i|^2M_i$LP, where F_i is the structure factor of reflection i, M_i the multiplicity factor of the reflection i in fiber diffraction patterns, and LP the Lorentz-polarization factor, accounting for the presence of the monochromator.[27b]

Simulated X-ray fiber diffraction patterns have been obtained using the software package[28] CERIUS^2 using isotropic thermal factor $B = 12$ Å^2 and fixing the half-width at half-height of crystallite orientation distribution (taken to be a Gaussian function centered on the fiber axis) equal to 7.6°.

Conformational and packing energy calculations were performed with the software package[28] CERIUS^2 using the force field PCFF[29] in the CERIUS program. For the conformational energy calculations on isolated molecules, a cutoff distance of 4 Å for attractive nonbonded interactions and for Coulombic interactions (dielectric constant, $\epsilon = 1$) was selected, and a spline function was used from 4 to 5 Å to attenuate gradually the interaction energy from its full value to zero. No interaction over 5 Å was taken into account.

Results and Discussion

Diffraction Data Analysis. The X-ray powder diffraction profile of as-prepared ECC sample is reported in Figure 1 (solid line); the amorphous contribution is also indicated (dashed line).

The degree of crystallinity, evaluated as the ratio of the integrated area of the Bragg diffraction and the area of the whole diffraction profile, amounts to ~56%. The most intense reflections of crystalline ECC sample (Figure 1) occur at $2\theta = 15.28°$, 18.15°, and 20.40° ($d =$ 5.80, 4.89, and 4.35 Å), in agreement with the X-ray powder diffraction pattern of ECC sample prepared with vanadium-based anionic coordination catalysts in ref 9b.

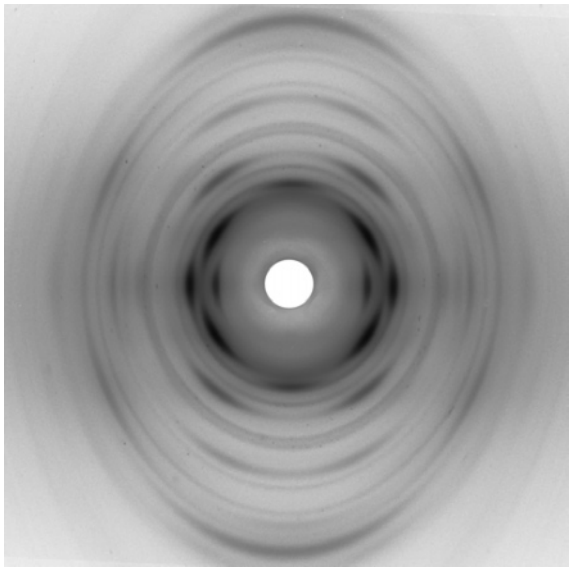

Figure 2. X-ray fiber diffraction pattern of oriented fiber of the ECC sample (Cu $K\alpha_1$, graphite single-crystal monochromator).

The X-ray fiber diffraction pattern of the stretched fiber of the sample ECC is reported in Figure 2. The reflections observed in the X-ray powder diffraction profile of Figure 1 are listed in Table 1 and compared with the reflections observed in the X-ray fiber diffraction pattern of Figure 2.

It is apparent that the X-ray fiber diffraction pattern of ECC fiber (Figure 2) presents the same reflections observed in the powder profile of the as-prepared sample (Figure 1). Moreover, the fiber pattern clearly shows that the first and third intense reflections at $2\theta = 15.28°$ and 20.40° in the powder diffraction pattern occur on the equator, whereas the strong reflection at $2\theta = 18.15°$ occurs on the first layer line (Table 1 and Figure 2).

From the X-ray fiber diffraction pattern a value of the chain axis period of 9.0 Å has been evaluated, in agreement with the chain axis period estimated from X-ray pattern of stretched fibers of early Natta's ECC samples.[9,10] The presence of a strong meridional reflection on the second and fourth layer line indicates inclusion of two ethylene and two cyclopentene units in the chain axis period.

All the reflections observed in the X-ray fiber and powder diffraction patterns are accounted for by the orthorhombic unit cell with axes $a = 7.83$ Å, $b = 8.76$ Å, and $c = 9.0$ Å. According to this unit cell, the two strong equatorial reflections at $d = 5.80$ and 4.35 Å and the strong reflection on the first layer line at $d = 4.89$ Å are indexed as 110, 020, and 111, respectively. This unit cell is in agreement with that one proposed by Corradini et al. in 1962 for the alternating isotactic ECC.[10a,b] The calculated crystalline density is 1.033 g/cm^3 for two ECC chains included in the unit cell, in agreement with the experimental density of 1.03 g/cm^3, measured by flotation on a sample having 56% crystallinity.

Geometrical Analysis. The chain structure of alternating copolymers of ethylene with olefins having internal double bonds is characterized by the presence of two chiral centers per monomeric unit, leading to

Table 1. Diffraction Angles (2θ), Bragg Distances (d), Cylindrical Reciprocal Coordinates (ξ and ζ), and Intensities (I_o) of the Reflections Observed on the Layer Lines l of the X-ray Fiber Diffraction Pattern of ECC Fiber of Figure 2, Compared with the Diffraction Angles, Bragg Distances, and Intensities Observed in the X-ray Power Diffraction Profile of Figure 1; Miller Indices of Reflections Are Also Indicated[a]

fiber pattern (Figure 2)						powder profile (Figure 1)			
2θ (deg)	d (Å)	ξ (Å^{-1})	ζ (Å^{-1})	l	I_o	2θ (deg)	d (Å)	I_o	hkl
15.17	5.84	0.171	0	0	s	15.28	5.80	64	110
20.23	4.39	0.228	0	0	vs	20.40	4.35	138	020
22.50	3.95	0.253	0	0	vw	22.95	3.87	37	200
30.23	2.96	0.338	0	0	w				220
33.12	2.70	0.370	0	0	w				130
35.62	2.52	0.397	0	0	m	35.62	2.52	36	310
18.06	4.91	0.171	0.111	1	vs	18.15	4.89	166	111
19.72	4.50	0.	0.221	2	ms				002
24.98	3.56	0.173	0.221	2	ms	25.06	3.55	64	112
						28.55	3.13	29	022
						29.91	2.99	23	202
38.48	2.34	0.366	0.221	2	w	38.90	2.31	30	132
33.49	2.68	0.169	0.333	3	m	33.70	2.66	42	113

[a] Key: vs = very strong; ms = medium strong; s = strong; m = medium; w = weak; vw = very weak.

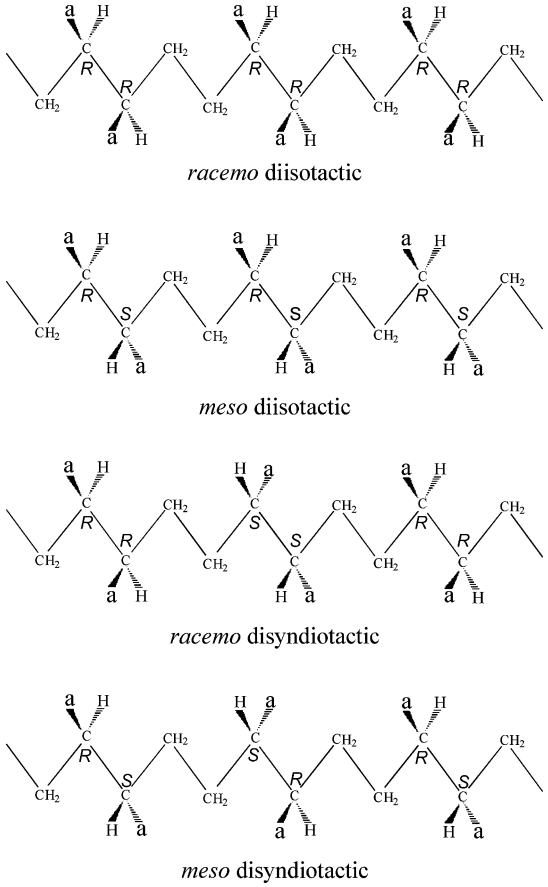

Figure 3. Four limit microstructures of ditactic vinyl polymer chains of maximum configurational order. "a" indicates a substituent unit, different from hydrogen.

ditactic structures. The ditactic structures are related to the relative configuration of adjacent asymmetric tertiary carbon atoms (*meso* or *racemo*) and to the relative configuration of successive units along the chain (isotactic or syndiotactic). "*Meso*" and "*racemo*" configurations correspond to a *cis* and *trans* opening of the internal double bond of a *cis*-olefin, respectively. The four limit microstructures, corresponding to a different succession of configuration of the tertiary carbon atoms, are shown in Figure 3.[30]

The configuration of two adjacent chiral carbon atoms in each E−C−E unit for a *meso*-ditactic chain can be only *R*/*S* or *S*/*R* (Figure 3). The *meso*-diisotactic microstructure of our alternating ECC sample thus corresponds to a regular succession of the tertiary carbon atoms according to the sequence $(RS)_n$ or $(SR)_n$ (Figure 3).

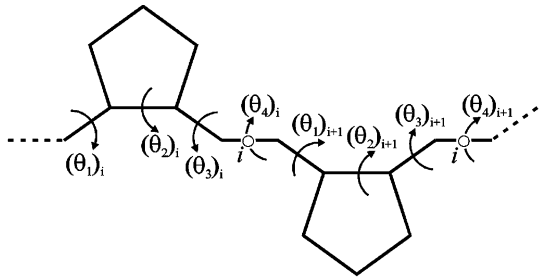

$(\theta_1)_i$	$(\theta_2)_i$	$(\theta_3)_i$	$(\theta_4)_i$	$(\theta_1)_{i+1}$	$(\theta_2)_{i+1}$	$(\theta_3)_{i+1}$	$(\theta_4)_{i+1}$	
θ_1	θ_2	θ_3	θ_4	θ_1	θ_2	θ_3	θ_4	**s**(M/N)
θ_1	θ_2	θ_3	T *i*	$-\theta_3$	$-\theta_2$	$-\theta_1$	T *i*	**t***i*
θ_1	*cis* *m*	$-\theta_1$	T *i*	θ_1	*cis* *m*	$-\theta_1$	T *i*	**s**(2/1)*m*

Figure 4. Line repetition symmetry groups and corresponding sequences of torsion angles for a chain of *meso*-diisotactic alternating ethylene−cyclopentene copolymer. The positions of the mirror planes (m) and inversion centers (i) along the polymer chain are also indicated.

The conformation of the chain in the crystalline state may be defined, using the equivalence principle,[30,31] in terms of its symmetry, which must be compatible with the chemical constitution and configuration. The possible line repetition groups for ECC chains compatible with the isotactic configuration are reported in Figure 4.

The helical repetition is compatible for the isotactic chain; the line repetition group is **s**(M/N) and corresponds to a succession of torsion angles $(\theta_1\theta_2\theta_3\theta_4)_n$. The *meso*-diisotactic polymer chain may also present inversion centers in the middle of the CH_2-CH_2 bonds of the ethylene units and mirror planes perpendicular to the chain axis, crossing the CH−CH bond of the cyclopentene ring. As a consequence, line repetition groups **t***i* (if only the inversion centers are present) and **s**(2/1)*m* (if both inversion centers and mirror planes are present) are also possible for the *meso*-diisotactic chain (Figure 4).

Chart 1. Puckered Conformation of Cyclopentane

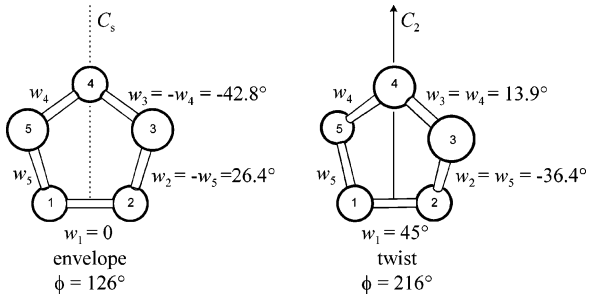

Chart 2. (1*R*,2*S*)-Diethylcyclopentane Used as Model Moecule for the Energy Calculations

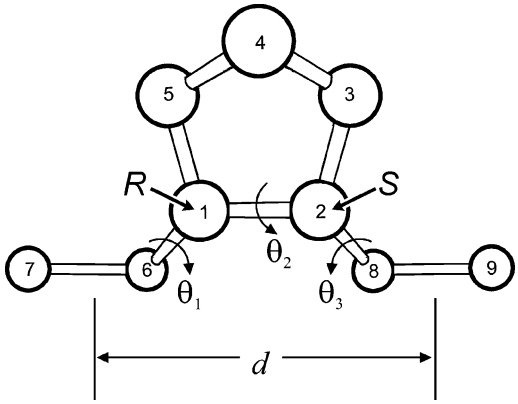

The **t***i* symmetry of the isotactic chain corresponds to a succession of torsion angles $(\theta_1\theta_2\theta_3\mathrm{T}-\theta_3-\theta_2-\theta_1\mathrm{T})_n$. The **s**(2/1)*m* symmetry of the isotactic chain corresponds to a succession of torsion angles $(\theta_1\ cis\text{-}\theta_1\ \mathrm{T})_n$. The value of the experimental chain periodicity $c = 9.0$ Å of ECC found by X-ray fiber diffraction pattern suggests nearly extended chains with a repetition occurring after two monomeric EC units. This is compatible with both **t***i* and **s**(2/1)*m* symmetries for the isotactic chain.

Conformational Energy Analysis. Conformational Analysis of Cyclopentane. The conformational analysis of alternating isotactic ethylene−cyclopentene copolymer has been started testing the PCFF[29] force field in the software package CERIUS[28] in the case of cyclopentane to compare the results of our calculations with those reported in the literature. Then the analysis has been extended to the *cis* isomer of 1,2-diethylcyclopentane ((1*R*,2*S*)-diethylcyclopentane or (1*S*,2*R*)-diethylcyclopentane) and finally to dimeric units of ECC in the *meso*-diisotactic configuration.

It is well-known that cyclopentane exhibit a nonplanar (puckered) conformation with dihedral angles largely deviating from zero. The potential energy surface of cyclopentane is very flat, and the ring freely pseudorotates between twist and envelope forms (having C_2 and C_s symmetry, respectively)[32−38] (see Chart 1).

To describe the pseudorotation phenomenon, the following expression for the torsion angles, w_k, was proposed:[33−39]

$$w_k = w_0 \cos(4\pi Ck/5 + \phi) \qquad k = 1, 2, 3, 4, 5 \quad (1)$$

where w_0 is the puckering amplitude, C the conversion factor from radians to degrees, and ϕ the phase angle of puckering. Conformations described by ϕ values equal to 0°, 36°, 72°, ... correspond to twist forms with C_2 symmetry; those described by ϕ values of 18°, 54°, 90°, ... correspond to envelope forms with C_s symmetry. As

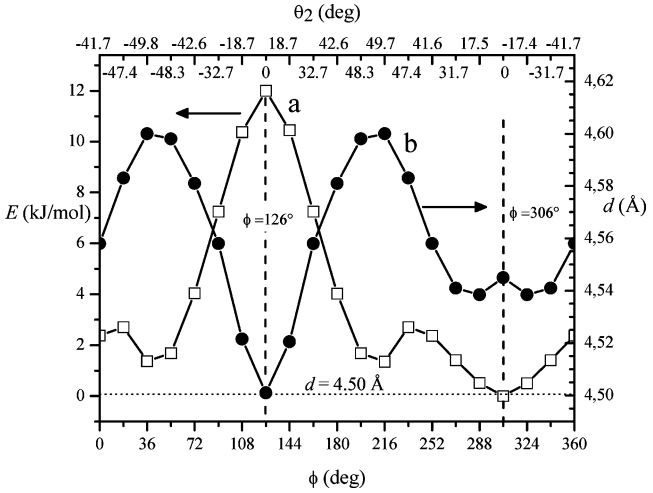

Figure 5. Values of the calculated energy E (a) and distance d (b), as defined in Chart 2, of (1*R*,2*S*)-diethylcyclopentane as a function of the phase angle ϕ defining the puckering of cyclopentane ring along the pseudorotational circuit according to eq 1. The value of the dihedral angle θ_2 for each conformer along the ϕ path is indicated in the upper abscissa axis in a nonlinear scale. The experimental value of the halved chain axis periodicity of the alternating diisotactic ECC ($c/2 = 4.50$ Å) is also indicated (dotted line).

ϕ varies from 0° to 360°, the structure goes through all possible C_2 and C_s forms.

In our calculations, the energy minima correspond to values of w_o equal to 45° in eq 1 (see Chart 1). These results compare well with those reported in the literature.[32,34,36,40] The energy difference between the C_s and C_2 structures is negligible, and the energy profile along the pseudorotational path connecting the C_s and C_2 conformations, obtained by energy minimization of several conformations of no symmetry, is practically flat.[41]

Conformational Energy Analysis of *cis*-1,2-Diethylcyclopentane. Conformational energy calculations have been performed on the *cis* isomer of -(1*R*,2*S*)-diethylcyclopentane for all possible envelope and twist conformations of the five-membered ring generated by eq 1 with $w_0 = 45°$ as a function of phase angle ϕ (i.e., in the ϕ range 0−360°, at step of 18°). For each conformation of the five-membered ring of (1*R*,2*S*)-diethylcyclopentane, the calculated energy has been optimized with respect to all internal variables in the diethyl moieties (bond angles and torsion angles θ_1, θ_2, and θ_3 shown in Chart 2) while keeping the conformation of the ring fixed, starting from the conformer with $\theta_1 = \theta_3 = 180°$ (see Chart 2).

The calculated values of energy E are reported in Figure 5 (curve a) as a function the phase angle ϕ (lower abscissa axis). In Figure 5, the value of the dihedral angle external to the five-membered cycle, $CH_2(6)-CH(1)-CH(2)-CH_2(8)$ (θ_2 in Chart 2), for each conformer (after minimization of internal energy), is indicated in the upper abscissa axis, whereas the corresponding dihedral angle $CH_2(5)-CH(1)-CH(2)-CH_2(3)$ internal to the ring is given by eq 1, with $k = 1$ (w_1). The distance between the middle of the two terminal CH_3-CH_2 bonds for each minimum energy conformer (d, see Chart 2) is also reported in Figure 5 (curve b).

It is apparent that the presence of the diethyl substituents removes the energy degeneration of the envelope and twist conformations typical of cyclopentane: the interconversion barriers among the various

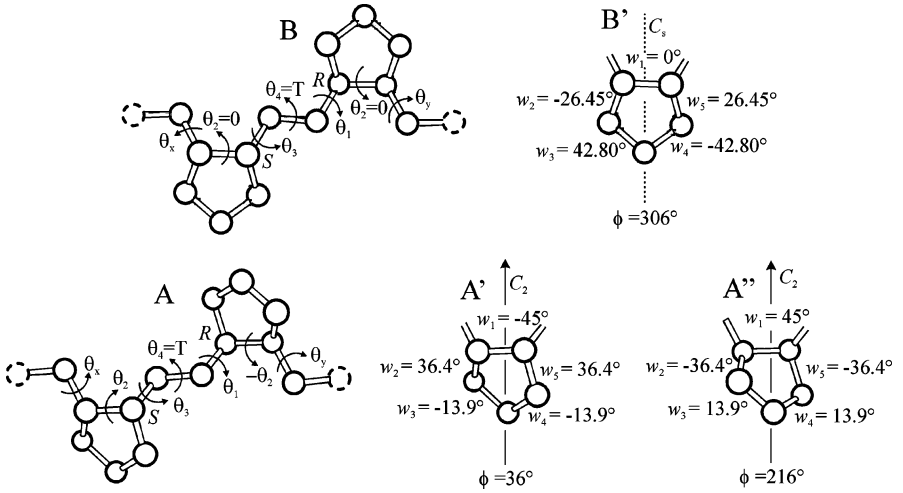

Figure 6. Portions of isolated *meso*-diisotactic chains of ethylene−cyclopentene copolymer including (A) the enantiomeric pair of cyclopentane rings in twist conformation given by $\phi = 36$ (A′) and 216° (A″) and (B) cyclopentane rings in envelope conformation corresponding to $\phi = 306°$ (B). The regular repetition of units of kind A with $\theta_1 = -\theta_3$, $\theta_x = -\theta_y$, and $\theta_4 = \mathrm{T}$ corresponds to the line repetition group $\mathbf{t}i$; the regular repetition of units of kind B with $\theta_1 = -\theta_3$, $\theta_x = -\theta_y$, $\theta_4 = \mathrm{T}$ and $\theta_2 = 0$ corresponds to the line repetition group $\mathbf{s}(2/1)m$. The *R*, *S* configuration of tertiary carbon atoms is also indicated.

conformers being nearly 12 kJ/mol for the 1,2-disubstituted cyclopentane.

The values of the dihedral angles $|\theta_1|$ and $|\theta_3|$ are in all cases comprised in the range +170° to 180° (see Supporting Information, Table S1), independent of the conformation of the ring. On the contrary, the dihedral angle θ_2 spans a wide range of values (from −50° to +50°) dependent on the phase angle ϕ. Couples of conformers equidistant along ϕ from the vertical bar at $\phi = 126°$ (306°) correspond to enantiomeric pairs. The whole ϕ path of (1*R*,2*S*)-diethylcyclopentane includes nine enantiomeric pairs, five with the ring in the twist conformation and four with the ring in the envelope conformation, in addition to the two singular envelope conformers corresponding to $\phi = 126°$ and 306°, which are not enantiomers. The envelope conformations with $\phi = 126°$ and 306° correspond to $\theta_2 = 0°$ and present the feature that the local C_s symmetry of the five-membered ring is maintained also for the 1,2-disubstituted compound. However, they are not isoenergetic; the conformer with $\phi = 306°$ corresponds to the absolute minimum-energy conformation, whereas the model with $\phi = 126°$ presents the highest energy (∼12 kJ/mol higher than the absolute minimum). Relative minima, 1.5 kJ/mol higher than the absolute minimum, occurs for the enantiomeric pair twist conformers with $\phi = 36°$ ($\theta_2 = -49.8°$) and 216° ($\theta_2 = 49.8°$); also in this case, the local C_2 symmetry of the ring is maintained for the whole molecule.

The *d* values for all conformers span the range 4.60−4.50 Å and are close to one-half the experimental chain periodicity of the alternating diisotactic ECC ($c/2 = 9.0/2$ Å). It is worth noting that, owing to the low-energy barrier of interconversion among the various conformers of *cis*-(1,2)-diethylcyclopentane (∼12 kJ/mol), all the conformations along the ϕ coordinate are practically accessible at room temperature, with a low cost of internal energy and a neat favorable entropic contribution to the free energy.

Conformational Analysis of Alternating Isotactic ECC. Conformational energy calculations have been performed on the portions of isolated *meso*-isotactic chain shown in Figure 6, corresponding to a dimeric unit of the alternating diisotactic ECC.

With reference to Figure 6, conformational energy maps have been calculated as a function of the dihedral angles, θ_1 and θ_3. The calculated energy for each point of the map has been minimized with respect to all internal variables, but those of the five-membered rings, starting from the conformation with the dihedral angles in the terminal ethyl groups (θ_x and θ_y) and θ_4 in the *trans* state. The latter condition arises from the need to consider only the conformations producing sufficiently extended chain oligomers after minimization, similar to the conformation of the alternating ECC chains in the crystalline state. The internal ring variables have been fixed equal to those found in the case of (1,2)-diethylcyclopentane along the ϕ path (Figure 5). The value of $|\theta_2|$ of the starting conformations depends on the conformation of the five-membered rings, variable in the range −50° to +50° along the ϕ path (Figure 5), defined in correspondence to the dihedral angle w_1. For the sake of simplicity, only the results for the models with the rings in the minimum energy twist conformation corresponding to the enantiomeric pairs with $\phi = 36°$ and 216° (Figure 6A) and the model with both rings in the minimum energy envelope conformation with $\phi = 306°$ (Figure 6B) are illustrated.

Maps of the conformational energy as a function of θ_1 and θ_3 are reported for the model oligomers of Figure 6A,B in Figure 7A,B, respectively. In both cases, the absolute minimum of the conformational energy occurs at $\theta_1 = -175°$, $\theta_3 = +175°$; relative minima are also present corresponding to $\theta_1 \approx -175°$, $\theta_3 \approx 95°$ and $\theta_1 \approx -95°$, $\theta_3 = 175°$. The minimization procedure at each point of the (θ_1, θ_3) map, in the regions of low energy, converges to values of $\theta_x \approx \theta_1$, $\theta_y \approx -\theta_1$, θ_4 close to 180° and to values of θ_2 close to those of the initial state; more precisely, $|\theta_2| = 49.8°$ for the model of Figure 6A including rings in twist conformation with $\phi = 36°$ and 216°, $\theta_2 = 0°$ for the model of Figure 6B including rings in envelope conformation with $\phi = 306°$. Therefore, the minimum-energy conformations of the models of Figure 6 correspond to nearly extended conformations, with a succession of dihedral angles θ_x, θ_2, θ_3, θ_4, θ_1, $-\theta_2$, θ_y close to −175°, −49.8, +175°, 180°, −175°, +49.8°, +175° for the model of Figure 6A and −175°, 0°, +175°, 180°, −175°, 0°, +175° for the model of Figure 6B. For

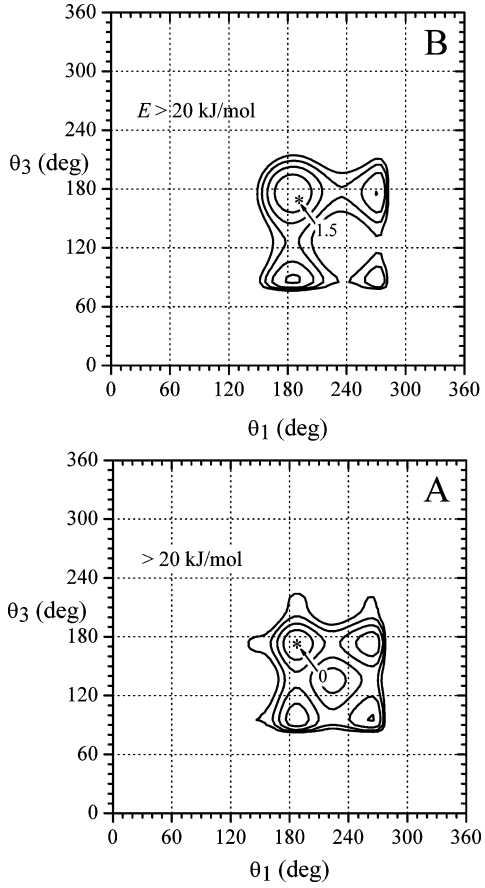

Figure 7. Maps of the conformational energy as a function of the torsion angles θ_1 and θ_3, for models of alternating isotactic ECC chains of Figure 6A including the enantiomeric pairs of cyclopentene rings in twist conformation given by $\phi = 36°$ and 216° (A) and of Figure 6B with cyclopentene rings in envelope conformation corresponding to $\phi = 306°$ (B). The curves are reported at intervals of 5 kJ/mol of EC units with respect to the absolute minimum of the map A assumed as zero. The value of the energy of the minimum of the map B, with respect to the absolute minimum is also reported.

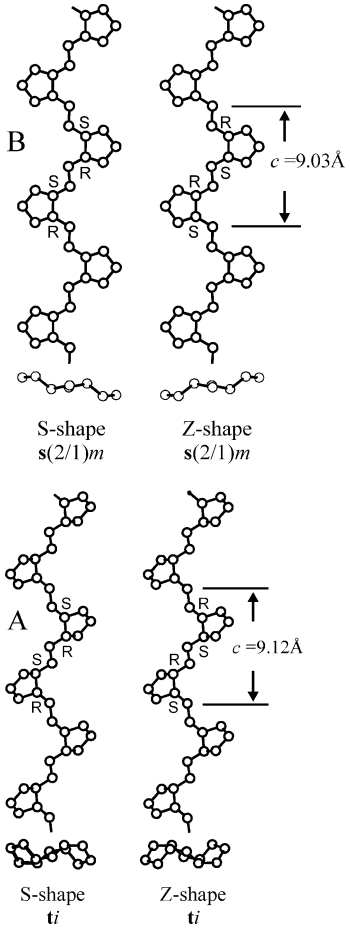

Figure 8. Side view and projection along the chain axis of the minimum-energy conformations in **t***i* (A) and **s**(2/1)*m* (B) symmetries of alternating diisotactic ECC. The chain conformation is $(T_3G^+ T_3G^-)_n$ for the **t***i* symmetry, $(T_3 \text{ cis } T_3 \text{ cis})_n$ for the **s**(2/1)*m* symmetry (B). The configuration of chiral carbon atoms in a repeating unit is indicated. The value of chain repetition unit, *c*, is also indicated. The sequence of configurations of tertiary carbon atoms in consecutive cyclopentene rings may be $(RS)_n$ or $(SR)_n$, yielding a projection along the chain axis characterized by S- or Z-shape.

both models the distance between the centers of the two CH_3-CH_2 terminal bonds is close to the experimental chain periodicity, $c = 9.0$ Å, of the alternating diisotactic ECC sample in the crystals. Furthermore, both models in the lowest energy conformer imply the presence of an inversion center in the middle of the CH_2-CH_2 bond of the ethylene unit.

Similar results have been obtained by performing conformational energy calculations on other model dimers of the alternating diisotactic ECC chain, including different couples of conformational enantiomeric pairs taken along the ϕ path of Figure 5.

The regular enchainment of enantiomeric couples of cyclopentene units of the kind shown in Figure 6A according to the sequence $(RS)_n$ of the stereoisomeric centers is compatible with the **t***i* symmetry for the infinite chain (Figure 4). Low-energy conformations of isotactic alternating ECC chain correspond to nearly extended conformations with a succession of backbone torsion angles of the kind (with reference to Figure 6A) $(\theta_3, \theta_4, \theta_1, -\theta_2, \theta_y, \theta_4, \theta_x, \theta_2)_n \equiv (+175°, 180°, -175°, -\theta_2, +175°, 180°, -175°, +\theta_2)_n$. The value of $|\theta_2|$ for the conformations of low energy of the ECC chains depends on the conformation of the five-membered rings and is variable in the range −50° to +50° along the ϕ path, defined in correspondence to the dihedral angle w_1 internal to the ring. The model of minimum-energy conformation of the alternating diisotactic ECC in the **t***i* symmetry having the rings in twist conformation corresponds to $|\theta_2| = 49.8°$ and therefore the succession $(T_3G^+T_3G^-)_n$ and is shown in Figure 8A in two projections parallel and perpendicular to the chain axis. The chain axis period *c* for this model is 9.12 Å, in agreement with theexperimental chain periodicity $c = 9.0$ Å of the alternating diisotactic ECC sample.

The regular enchainment of units of the kind shown in Figure 6B according to the sequence $(RS)_n$ of the stereoisomeric centers is compatible with the **s**(2/1)*m* symmetry for the infinite chain (Figure 4). The model conformations for the alternating diisotactic ECC in the **s**(2/1)*m* symmetry corresponds to nearly extended conformations with a succession of the backbone torsion angles of kind (with reference to Figure 6B) $(\theta_3, \theta_4, \theta_1, \text{cis})_n \equiv (+175°, 180°, -175°, 0)_n$. This symmetry may occur only for the ring in envelope conformations identified by the phase angle $\phi = 306°$ and 126°, since only in these cases $\theta_2 = 0$ (Figure 5). Furthermore, whereas the **s**(2/1)*m* model conformation built up using the rings with $\phi = 306°$ corresponds indeed to a minimum-energy conformation, the model conformation for $\phi = 126°$ is ∼12 kJ/mol (EC unit) higher than the

lowest minimum.

The model of minimum-energy conformation $(T_3\ cis)_n$ of the alternating diisotactic ECC in the **s**(2/1)*m* symmetry with the rings in envelope conformation having $\phi = 306°$ is shown in Figure 8B in two projections parallel and perpendicular to the chain axis. Also in this case the chain periodicity, $c \approx 9.03$ Å, is in agreement with the experimental chain axis period of ECC in the crystalline state.

In conclusion, whatever the conformation of the rings, nearly extended conformations of alternating isotactic ECC chain in the **t***i* symmetry may be built up, through the regular enchainment of enantiomeric pairs conformers of cyclopentene rings along the ϕ path of Figure 5, with a sequence of the backbone torsion angles of the kind $(T_3\ \theta_2\ T_3\ -\theta_2)_n$ and θ_2 variable in the range −50° to +50°. All conformations have low internal energy and have periodicity close to the experimental value of the chain axis periodicity. Conformations of **s**(2/1)*m* symmetry corresponding to sequences $(T_3\ cis)_n$ are also suitable, although this symmetry is more restrictive as far as the number of independent variable and the conformations of the rings.

The chain of the alternating diisotactic ethylene/cyclopentene copolymer has a directional property due to the fact that the configuration of tertiary carbon atoms in consecutive cyclopentene rings may be either $(RS)_n$ or $(SR)_n$ The different successions of configurations produce different stereo-orientations of the chain and different projections along the chain axis, characterized by different shapes of the chain, S-shape or Z-shape, as shown in Figure 8.

The chain conformation of the alternating isotactic ECC in the crystalline state corresponds to the regular succession of enantiomorphic, anticlined structural units instead of a helical repetition of isomorphous isoclinic structural units as generally occurs for isotactic vinyl polymers. The $(T_3G^+T_3G^-)_n$ conformation of ECC copolymer is similar to the chain conformation of the alternating diisotactic ethylene−*cis*-2-butene copolymer in the crystals,[10] and both represent rare examples of isotactic vinyl polymer, which do not adopt a helical conformation in the crystalline state.[42]

It is worth noting that it is possible to build up nearly extended, disordered conformations of the alternating diisotactic ECC, through the random enchainment of enantiomeric or even not enantiomeric pair conformers of 1,2-substituted cyclopentane taken along the ϕ path of Figure 5; these chain conformations would be at low cost of internal energy and would present average periodicity close to 9.0 Å, provided that the main chain conformation is of the kind $...T_3\theta_iT_3\theta_{i+1}T_3\theta_{i+2}T_3\theta_{i+3}$ with $...\theta_i,\ \theta_{i+2}...$ variable in the range 0 to +50° and $...\theta_{i+1},\ \theta_{i+3}...$ variable in the range 0 to −50° depending on the conformation of the ring. A disordered conformation of the alternating diisotactic ECC of low energy, including cyclopentene rings in envelope, twist, and any intermediate conformation is shown in Figure 9; the average chain periodicity, $c \approx 9.0$ Å, is in agreement with the experimental chain axis periodicity of ECC in the crystalline state.

Crystal Structure. The calculations of the packing energy of ECC chains in various space groups and of the corresponding structure factors are described in detail only for chains of **t***i* and **s**(2/1)*m* symmetries of parts A and B of Figure 8, respectively. Without loss of generality, only space groups that maintain all the symmetry elements of the chains as crystallographic symmetry have been considered in the present calculations. The presence of the two strong 110 and 020 equatorial reflections (at $d = 5.80$ and 4.35 Å), and of the strong 111 reflection on the first layer line (at $d = 4.89$ Å) in the diffraction patterns of Figures 1 and 2 (Table 1), suggests a packing mode of ECC chains with the chain axes positioned at (0 0 *z*) and ($^1/_2$ $^1/_2$ *z*) of the unit cell.

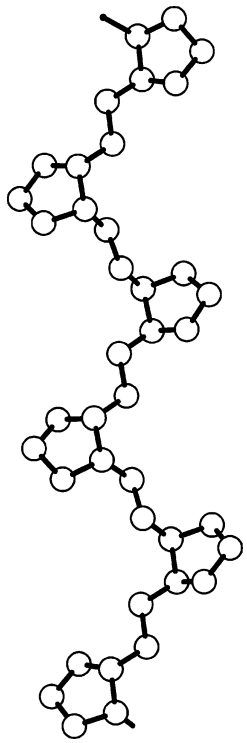

Figure 9. Extended, disordered conformation of the alternating diisotactic ECC of low internal energy, characterized by the random enchainment of conformers of 1,2-substituted cyclopentane taken along the ϕ path of Figure 5. The average periodicity is close to 9.0 Å. The main chain conformation is of the kind $...T_3\theta_iT_3\theta_{i+1}T_3\theta_{i+2}T_3\theta_{i+3}...$ with $...\theta_i,\ \theta_{i+2}...$ variable in the range 0 to +50° and $...\theta_{i+1},\ \theta_{i+3}...$ variable in the range 0 to −50° depending on the conformation of the ring.

Possible models of packing for ECC chains in **t***i* and **s**(2/1)*m* symmetries consistent with the above assumptions and corresponding to the space groups $P2_1/a$, $P2_1/n$, and *Pnam* are shown in Figure 10. All considered packing models are centrosymmetric and are characterized by two chains in the orthorhombic unit cell. The local inversion center of the chains placed in the middle of $-CH_2-CH_2-$ bonds of the ethylene units coincides with the crystallographic inversion centers of the considered space groups; furthermore, for the chains in **s**(2/1)*m* symmetry, the local 2-fold axis and the mirror planes *m* of the chains coincide with equivalent crystallographic elements of symmetry of the space group.

In the models of Figure 10A,C *ac* layers of chains in the **t***i* and **s**(2/1)*m* conformations, respectively, having alternatively Z- and S-shapes are piled along *b* and shifted by **a**/2 according to the space group $P2_1/a$ (*b* unique axis) (Figure 10A) and *Pnam* (Figure 10C). The limit ordered model of packing shown in Figure 10B is similar to that one of Figure 10A, but the chains, in the **t***i* conformation, have the same Z- or S-shape (space group $P2_1/n$, *c* unique axis).

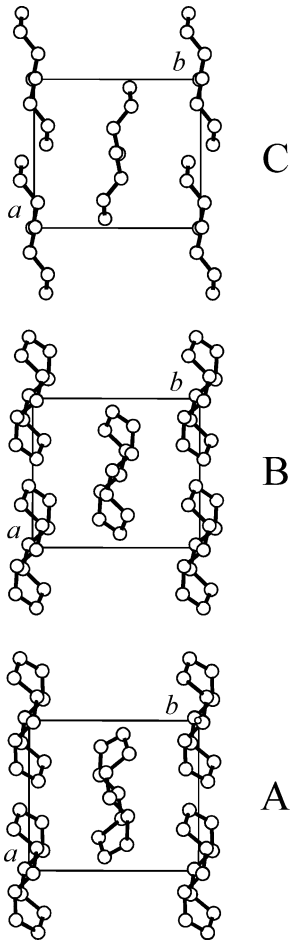

Figure 10. Limit ordered models of packing of alternating diisotactic ECC chains in the orthorhombic unit cell and space groups $P2_1/a$ (A), $P2_1/n$ (B), and *Pnam* (C). In the models $P2_1/a$ (A) and $P2_1/n$ (B) chains in the **t***i* symmetry conformation having S- and Z-shapes or the same S- and Z-shape, respectively, are included in the unit cell. In the model *Pnam* (C) chains in the **s**(2/1)*m* conformation having S- and Z-shapes are included in the unit cell.

The asymmetric unit corresponds to a single EC constitutional unit (one-half of the repeating unit) for the monoclinic space groups $P2_1/a$ and $P2_1/n$ and to one-half EC constitutional unit for the orthorhombic *Pnam* space group. The orientations of the chains in the models of Figure 10 have been found by minimizing the packing energy with respect to the rotation of the chains around the chain axis. The packing models of Figure 10A−C correspond to minima of the lattice energy; they present similar orientation of the chains, independent of the symmetry of the unit cell. In all cases the distances between couples of nonbonded atoms are equal to or greater than the sum of their atomic van der Waals radii.

Fractional coordinates and occupancy factors of the carbon atoms of the asymmetric units in the limit ordered models of Figure 10A (space group $P2_1/a$), Figure 10B (space group $P2_1/n$), and Figure 10C (space group *Pnam*) are reported in the Supporting Information (Table S2).

The calculated structure factors F_c for the three limit ordered models of Figure 10A−C are reported in Table 2 and compared with the observed structure factors F_o evaluated from the experimental intensities observed in the X-ray powder diffraction profile of Figure 1. In Table 3 the calculated intensities I_c for X-ray fiber diffraction patterns are compared with the experimental intensities I_o observed in the X-ray fiber diffraction pattern of Figure 2.

Although the data of Table 2 indicate that the calculated structure factors are in good agreement with the experimental intensities observed in the powder diffraction profile, inspection of the data of Table 3 indicate that some reflections, which are calculated with medium or low intensity, are not observed in the experimental fiber diffraction pattern of Figure 2 (for instance the 210, 230, 001, $\bar{1}21$, 012, $\bar{2}02$, $\bar{2}12$, $\bar{2}22$, 003, and $\bar{1}23$ reflections for the space group $P2_1/a$; the 310, 021, $1\bar{2}1$, $1\bar{3}1$, 012, and $2\bar{2}2$ reflections for the space group $P2_1/n$; the 120, 210, 230, 011, 121, and 113 for the space group *Pnam*).

This indicates that some additional disorder is present in the structure, besides the conformational disorder of cyclopentene rings which at room temperature interconvert between twist and envelope conformations with a low cost of internal energy. A possible disorder may be related to the statistical substitution of chains having S- and Z-shape, in each site of the lattice. Limit disordered models characterized by this kind of statistical disorder, shown in Figure 11, may be described by the statistical space groups *Pcan* for the chains in the **t***i* conformation (Figure 11A) and *Ccmm* for the chains in **s**(2/1)*m* conformation (Figure 11B). This statistical substitution is feasible because two chains with S- and Z-shape have the atoms of cyclopentene ring approximately in the same positions, according to an ideal long-range order.

The calculated structure factors and intensities for the limit disordered models of Figure 11 are also reported in Table 2 (for the powder diffraction) and Table 3 (for the fiber diffraction), respectively. The agreement between calculated and observed intensities is noticeably improved by the presence of the S−Z disorder. In fact, as shown in Table 3, the 120, $\bar{2}10$, $\bar{2}30$, 011, 021, 121 (or $\bar{1}21$), 012, $\bar{2}02$, $\bar{2}12$, $\bar{2}22$ (or $2\bar{2}2$), $\bar{1}23$, 001, and 003 reflections, which are absent in experimental X-ray fiber diffraction pattern (Figure 2) and are calculated of low or medium intensity for the limit ordered model structures of Figure 10, are now calculated zero or with very low intensity for the limit disordered model structures of Figure 11.

The calculated X-ray fiber diffraction patterns for the limit disordered model structures of Figure 11 are compared with the experimental X-ray fiber diffraction pattern in Figure 12. Overall, the calculated patterns (Figure 12B,C) show a good agreement with the experimental X-ray diffraction intensity distribution. However, for the limit disordered model of isotactic ECC chains of **t***i* conformation and space group *Pcan* (Figure 11A) the intensity of 113 reflection is calculated too weak with respect the experimental value (Figure 12B and Table 3), whereas for the limit disordered model of isotactic ECC chains of **s**(2/1)*m* conformation and space group *Ccmm* (Figure 12B) a better agreement is obtained (Figure 12C and Table 3). Nevertheless, it is not possible to discriminate between the different structural models of disorder, since in the simplified models of Figure 11 the conformation of the rings has been assumed fixed. Since the cyclopentene rings easily interconvert between all possible twist and envelope conformers of the pseudorotational circuit of unsubstituted cyclopentane, the conformation of the chain is much

Table 2. Comparison between Observed Structure Factors (F_o), Evaluated from the Intensities Observed in the X-ray Powder Diffraction Profile of Figure 1, and Calculated Structure Factors (F_c) for the Limit Ordered Models of Packing of Alternating Isotactic ECC of Figure 10A (Space Group $P2_1/a$), Figure 10B (Space Group $P2_1/n$), and Figure 10C (Space Group *Pnam*), and for the Limit Disordered Models of Figure 11A (Space Group *Pcan*) and Figure 11B (Space Group *Ccmm*)[a]

						$F_c = (\sum\|F_i\|^2 M_i)^{1/2}$									
(*hkl*)	$2\theta_o$ (deg)	$2\theta_c$ (deg)	d_o (Å)	d_c (Å)	$F_o = (I_o/LP)^{1/2}$	$P2_1/a$ (**ti**)		$P2_1/n$ (**ti**)		*Pcan* (**ti**)		*Pnam* **s**(2/1)*m*		*Ccmm* **s**(2/1)*m*	
001		9.83		9.00		13		0		0					
011		14.11		6.28		8		11		0		36		0	
101	15.28	15.00	5.80	5.91	64	0	71	15	78	0		0	68	0	
1$\bar{1}$0		15.18		5.84		71		69		71		57		55	
$\bar{1}$10		15.18		5.84				30							
111						92		85		153		139		142	
$\bar{1}$11	18.15	18.11	4.89	4.90	166	124	153		153						
1$\bar{1}$1								125							
002		19.73		4.50		27		27		27		8		8	
020	20.40	20.27	4.35	4.38	138	119	121	117	121	119	121	130	130	130	130
012		22.21		4.00		21		25		21		0		0	
021		22.58		3.94		6		34		0		0		0	
200	22.95	22.71	3.87	3.91	37	7	28	10	44	7	22	7	41	8	
102		22.79		3.90		0		12		0		0		0	
120		23.27		3.82		16		0		0		41		0	
$\bar{2}$01		24.80		3.59		4		0		0		6		7	
201		24.80		3.59		4									
210		24.91		3.57		24		0		0		36		0	
1$\bar{1}$2		24.98		3.56		44		35		49		56		60	
$\bar{1}$12		24.98		3.56		26									
112		24.98		3.56				38							
121	25.06	25.31	3.55	3.52	64	4	83	20	69	39	63	52	85	0	60
$\bar{1}$21		25.31		3.52		60									
1$\bar{2}$1		25.31		3.52				38							
$\bar{2}$11		26.84		3.32		4		1		6		2		0	
2$\bar{1}$1		26.84		3.32		5									
2$\bar{1}$1		26.84		3.32				13							
022	28.55	28.44	3.13	3.14	29	10		15		10		3		1	
003		29.78		3.00		7		0		0		0		0	
202	29.91	30.26	2.99	2.95	22	12	36	28		32		12		15	
$\bar{2}$02		30.26		2.95		33									
220		30.63		2.92		24		41		24		17		17	
2$\bar{2}$0		30.63		2.92				1							
122		30.69		2.91		17		11		16		6		0	
$\bar{1}$22		30.69		2.91		7									
1$\bar{2}$2		30.69		2.91				18							
013		31.52		2.84		12		6		0		10		0	
103		31.95		2.80		0		8		0		0		0	
$\bar{2}$12		31.98		2.80		4		10		30		8		0	
2$\bar{1}$2		31.98		2.80		38									
212		31.98		2.84				29							
031		32.23		2.78		11		10		0		35		0	
$\bar{2}$21		32.24		2.78		2		3		0		13		13	
2$\bar{2}$1		32.24		2.78		2									
221		32.24		2.78				8							
130		32.73		2.74		35		33		35		55		54	
1$\bar{3}$0		32.73		2.74				4							
113	33.70	33.59	2.66	2.67	42	15	45	10	55	8	41	35	83	36	77
1$\bar{1}$3		33.59		2.67		3									
11$\bar{3}$		33.59		2.67				1							
$\bar{1}$31		34.25		2.62		7		12		19		37		38	
1$\bar{3}$1		34.25		2.62		21									
13$\bar{1}$		34.25		2.62				39							
301		35.82		2.51		0		10		0		0		0	
310		35.90		2.50		32		28		31		22		23	
3$\bar{1}$0		35.90		2.50				18							
023		36.29		2.47		5		16		0		0		0	
032	35.62	36.69	2.52	2.45	36	15	47	17	58	15	44	0	31	0	34
$\bar{2}$22		36.70		2.45		7		4		27		22		25	
2$\bar{2}$2		36.70		2.45		31									
222		36.70		2.45				40							
311		37.31		2.41		23		23		18		8		10	
3$\bar{1}$1		37.31		2.41		3									
31$\bar{1}$		37.31		2.41				7							
203		37.78		2.38		13		0		0		6		5	
2$\bar{0}$3		37.78		2.38		13									
123		38.13		2.36		10		11		29		7		0	
1$\bar{2}$3		38.13		2.36		31									
12$\bar{3}$		38.13		2.36				29							
230	38.90	38.46	2.31	2.34	30	30	59	0	59	0	43	45	54	0	24
132		38.51		2.34		19		25		26		20		22	
1$\bar{3}$2		38.51		2.34		18									
13$\bar{2}$		38.51		2.34				26							
213		39.20		2.30		1		15		1		17		0	
2$\bar{1}$3		39.20		2.30		3									
21$\bar{3}$		39.20		2.30				19							

[a] The Bragg angles ($2\theta_o$) and the Bragg distances (d_o) observed in the X-ray powder diffraction profile of ECC of Figure 1, and those calculated ($2\theta_c$ and d_c) are also reported. *hkl* are the indices of the reflections in the orthorhombic unit cell.

Table 3. Comparison between Experimental Intensities (I_o), Observed in the X-ray Fiber Diffraction Pattern of Figure 2, and Calculated Intensities (I_c) for the Limit Ordered Models of Packing of Isotactic ECC of Figure 10A (Space Group $P2_1/a$), Figure 10B (Space Group $P2_1/n$), and Figure 10C (Space Group *Pnam*)) and for the Limit Disordered Models of Figure 11A (Space Group *Pcan*) and Figure 11B (Space Group *Ccmm*)[a]

						$I_c = \sum\|F_i\|^2 M_i$ LP/100						
hkl	$2\theta_o$ (deg)	$2\theta_c$ (deg)	d_o (Å)	d_c (Å)	I_o[c]	$P2_1/a$ ti chain		$P2_1/n$ ti chain		*Pcan* ti chain	*Pnam* s(2/1)m chain	*Ccmm* s(2/1)m chain
{110						234		112				
{1$\bar{1}$0	15.17	15.18	5.84	5.84	s			22	134	117	75	70
020	20.23	20.27	4.39	4.38	vs	484		239		242	294	294
200	22.50	22.71	3.95	3.91	vw	1		2		1	1	1
120		23.27		3.82		7					26	
210		24.91		3.57		15					18	
{220						12		19		6	3	3
{2$\bar{2}$0	30.23	30.63	2.96	2.92	w			0	19			
{130						24		11		13	31	31
{1$\bar{3}$0	33.12	32.73	2.70	2.74	w			0	11			
{310						18		7		9	5	5
{3$\bar{1}$0	35.62	35.90	2.52	2.50	m			3	10			
230		38.46		2.34		15					17	
001		9.83		9.00		849		0				
011		14.11		6.28		2		2			23	0
101		15.00		5.91				4				
{111						196		84		271	229	238
{$\bar{1}$11	18.06	18.11	4.92	4.90	vs	360	556		266			
{1$\bar{1}$1								182				
021		22.58		3.94		1		10				
{121						0		3		11	20	
{$\bar{1}$21		25.31		3.52		53	53		14			
{1$\bar{2}$1								11				
031		32.23		2.78		1		1		0	7	0
{131						0		0		2	7	7
{$\bar{1}$31		34.25		2.62		4	4		8			
{1$\bar{3}$1								8				
{311						5		2		2	0	0
{$\bar{3}$11		37.31		2.41		0	5		2			
{3$\bar{1}$1								0				
002[b]	19.72	19.73	4.50	4.50	ms	3696		3696		3696	360	330
012		22.21		4.00		16		12		8		
{102								2				
{$\bar{1}$02		22.79		3.90								
{112						45		15		28	37	43
{$\bar{1}$12	24.98	24.98	3.56	3.56	ms	16	61		32			
{1$\bar{1}$2								17				
022		28.44		3.14		2		2		1	0	0
{202						2		6		8	0	2
{$\bar{2}$02		30.26		2.95		17	19					
{122						4		1		2	0	0
{$\bar{1}$22		30.69		2.91		1	5		3			
{1$\bar{2}$2								2				
{212						0		1		6	0	
{$\bar{2}$12		31.98		2.80		20	20		7			
{2$\bar{1}$2								6				
032		36.69		2.45		2		1		1		
{222						1		0		4	3	4
{$\bar{2}$22		36.70		2.45		11	11		9			
{2$\bar{2}$2								9				
{132						4		3		3	2	2
{$\bar{1}$32	38.48	38.51	2.34	2.34	w	3	7		6			
{1$\bar{3}$2								3				
{302								2				
{$\bar{3}$02		39.93		2.58								
003		29.78		3.00		270		0				
013		31.52		2.84		9		1			3	0
{103						0		2				
{$\bar{1}$03		31.95		2.80								
{113						6		1		1	17	17
{$\bar{1}$13	33.49	33.59	2.68	2.67	m	0	6					
023		36.29		2.47		0		2				
{203						3		0		0	0	0
{$\bar{2}$03		37.78		2.38		3	6					
{123						1		1		6	3	
{$\bar{1}$23		38.13		2.36		15	16		7			
{1$\bar{2}$3								6				
{213								2		0	2	
{$\bar{2}$13		39.20		2.30		0			4			
{2$\bar{1}$3								2				

[a] The Bragg angles ($2\theta_o$) and the Bragg distances (d_o) observed in the X-ray fiber diffraction pattern of ECC of Figure 2 and those calculated ($2\theta_c$ and d_c) are also reported. Only reflections having a calculated intensity higher than 100 are reported. *hkl* are the indices of the reflections in the orthorhombic unit cell. [b] The exact spacing of the 002 reflection has been obtained by collecting the diffracted intensity with the fiber in the tilted orientation, i.e., mounted with the fiber axis perpendicular to the axis of the cylindrical camera and to the incident X-ray beam, while oscillating the fiber by ± 20° around the axis of the cylindrical camera. [c] Key: vs = very strong; ms = medium strong; s = strong; m = medium; w = weak; vw = very weak.

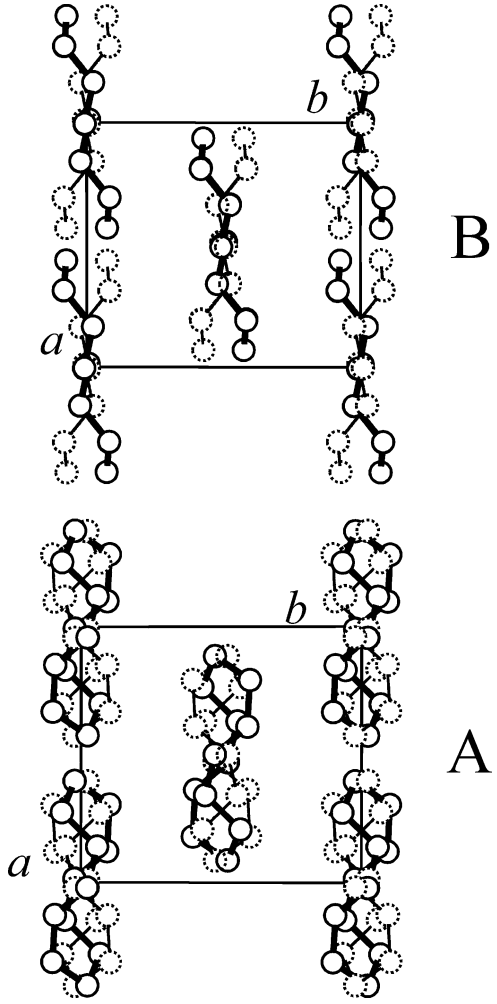

Figure 11. Limit disordered models, containing statistical S−Z disorder, of isotactic ECC chains of **t***i* (A) and **s**(2/1)*m* (B) conformations in the orthorhombic unit cell and space groups *Pcan* (A) and *Ccmm* (B). In each site of the lattice S- and Z-chains are present with the same probability.

more disordered than that assumed in our simplified models.

In conclusion, the present structural analysis indicates that the crystal structure of alternating diisotactic ethylene/cyclopentene copolymer is characterized by different kinds of disorder in the conformation and the packing of the chains. The conformational disorder is related to the cyclopentene rings, which interconvert, at low cost of internal energy, between all possible twist and envelope conformers of the pseudorotational circuit; the disorder in the packing derives from the statistical substitution of ECC chains in $(T_3G^+T_3G^-)_n$ or $(T_3\ \mathrm{cis})_n$ conformation with S- and Z-shape in the sites of the lattice.

Conclusions

A strictly alternating *meso*-diisotactic ethylene−cyclopentene copolymer has been prepared by ring-opening metathesis polymerization of bicyclo[3.2.0]hept-6-ene using a chiral molybdenum−carbene complex and successive hydrogenation of the unsaturated polymer. A model for the crystal structure of alternating ECC is proposed. Oriented fibers of ECC have been obtained, and the corresponding X-ray fiber diffraction pattern has been reported. A value of the chain axis of 9.0 Å has been evaluated. Geometrical and conformational

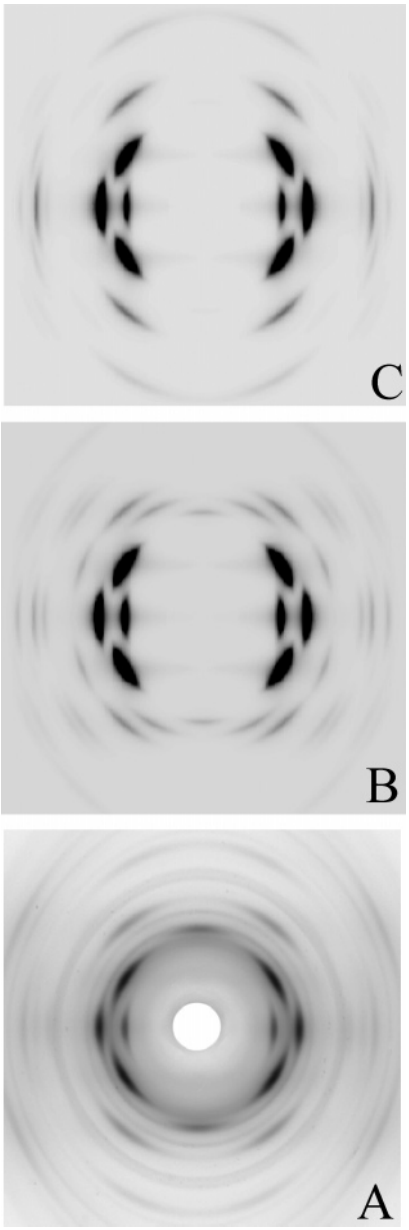

Figure 12. Comparison between calculated X-ray fiber diffraction pattern for the limit disordered models of Figure 11A (space group *Pcan*) (B) and Figure 11B (space group *Ccmm*) (C) and the experimental X-ray fiber diffraction pattern (A).

energy analyses have shown that isotactic ECC chains assume nearly extended conformations having **t***i* or 2-fold helical **s**(2/1)*m* symmetries corresponding to a repetition of anticlined enantiomorphic structural units along the chain and succession of backbone torsion angles $(T_3\theta_2\ T_3-\theta_2)_n$ and $(T_3\ \mathrm{cis})_n$, respectively. For the **t***i* conformation θ_2 is variable in the range −50° to +50° depending on the conformation of the ring. Both conformations account for the experimental chain axis of 9.0 Å.

The X-ray fiber and powder diffraction patterns are accounted for by models of packing of isotactic ECC chains in **t***i* and **s**(2/1)*m* conformations in the orthorhombic unit cell with axes $a = 7.83$ Å, $b = 8.76$ Å, $c = 9.0$ Å. Different kinds of structural disorder are present in the structure. The structural disorder is related to the cyclopentene ring that interconvert between twist and envelope forms at a low cost of internal energy (conformational disorder) and to the statistical substitu-

tion of chains having S- and Z-shape in each site of the lattice (statistical S−Z disorder).

The crystal structure can be described in terms of limit ordered models for several conformations of the chains, characterized by ideal long-range order and limit disordered models characterized by statistical S−Z disorder. Possible limit ordered models correspond to space groups $P2_1/a$ and $P2_1/n$ (for **t***i* chains) and *Pnam* (for **s**(2/1)*m* chains). Limit disordered models correspond to the statistical space groups *Pcan* (for **t***i* chains) and *Ccmm* (for **s**(2/1)*m* chains). The real crystalline modifications are probably intermediate between the limit ordered and the limit disordered models. Both the conformational disorder and statistical S−Z disorder may be simultaneously present in the structure. While the amount of S−Z structural disorder depends, probably, on the microstructure of the chains and on the condition of crystallization of the sample, the conformational disorder of the rings is always present, owing to the low interconversion barrier between twist and envelope conformations. This disorder is dynamic and may be reduced only at low temperature.

It is worth noting that disorder in the conformation of cyclopentene rings for ECC is analogous to the disorder described also for other crystalline polymers containing cyclopentane rings along the main chain, for instance poly(methylene-1,3-cyclopentane) (PMCP),[43,44] or as side groups, for instance isotactic poly(vinylcyclopentane).[45] In particular, independent of the microstructure of PMCP chains, similar crystalline structures are formed, characterized by hexagonal packing of the chain axes and a high degree of disorder as far as the rotation of the chains around the chain axes and the relative translation of the chains parallel to the axes. This disorder is linked either to disorder in the *cis* or *trans* configuration of cyclopentane rings or to the disorder in the relative chirality of consecutive stereoisomeric centers determining a different tacticity of PMCP chains.[43,44] In all cases, a high degree of dynamic disorder in the conformation of cyclopentane rings is present as in the case of ECC.[44] In the case of poly(vinylcyclopentane), instead, the conformational freedom of cyclopentane rings is restricted in a narrow range of the pseudorotational path, dictated by severe ring-to-chain steric interactions.[45]

The crystal structure of alternating ECC presents structural features also similar to the crystal structure of another important class of cyclic olefin copolymers, the alternating ethylene−norbornene copolymers (ENCs), in particular as far as the statistical occupancy of the lattice sites from chains having S- and Z-shapes is concerned.[8] However, other kinds of structural disorder are also present in the crystal structure of ENCs, depending on the degree of stereoregularity. The crystal structure of alternating ENCs is, indeed, mainly defined by the packing of the quasi-spherical norbornene units with the barycenters arranged on a face-centered orthorhombic or tetragonal lattice. In a limit disordered model of the crystal structure of alternating isotactic ENC disorder in the positioning of the carbon atoms of ethylene units is present which may connect with equal probability a given norbornene unit with any of its next neighbors.[8] The partial three-dimensional order which characterizes the crystal structure of ENCs is guided by the ordered positioning of the ball-like norbornene units and is obtained even though the polymers are configurationally disordered, provided that they have a regular alternation of the comonomeric units. In other terms, the origin of crystallinity in ENCs is basically due to the presence of alternating ethylene-norbornene sequences and, only marginally, to a stereoregular microstructure.

Probably also in the case of alternating ECCs the crystallinity is not linked to a strictly stereoregular isotactic microstructure. Strong indications that support this hypothesis are reported in ref 21 in the case of a poorly stereoregular, slightly syndiotactic, alternating ECC sample, and in ref 23 for an alternating atactic ECC sample. The low degree of stereoregularity of these samples, indeed, does not prevent the formation of crystals, although highly disordered, with melting temperatures (around 125 °C) lower than that of alternating isotactic ECC samples (185 °C).

The crystal structure of alternating ECC provides an example of the concept in polymer science that crystallinity may not be destroyed by the presence of high degrees of conformational, packing, and configurational disorder and the absence of long-range order.

Acknowledgment. Financial support from the "Ministero dell'Istruzione, dell'Università e della Ricerca" (PRIN 2004 project), and Sumitomo Chemicals is gratefully acknowledged.This work made use of the Cornell Center for Materials Research Shared Experimental Facilities, supported through the National Science Foundation Materials Research Science and Engineering Centers program (DMR-0079992).

Supporting Information Available: Method and conditions of preparation of ECC sample; tables showing the values of torsion angles θ_1 and θ_3 defined in Chart 2 as a function of phase angle of the ring (ϕ) and fractional coordinates of the asymmetric units in the proposed models of the crystal structure of ECC. This material is available free of charge via the Internet at http://pubs.acs.org.

References and Notes

(1) Kaminsky, W.; Arndt-Rosenau, M. In *Metallocene-Based Polyolefins*; Scheirs, J., Kaminsky, W., Eds.; Wiley: Chichester, 2000; Vol. 2, p 91.
(2) Kaminsky, W.; Arndt, M. *Adv. Polym. Sci.* **1997**, *127*, 143.
(3) Kaminsky, W.; Bark, A.; Arndt, M. *Macromol. Chem., Macromol. Symp.* **1991**, *47*, 83.
(4) Kaminsky, W. *Catal. Today* **2000**, *62*, 23. Kaminsky, W.; Laban, A. *Appl. Catal., A* **2001**, *222*, 47.
(5) Ruchatz, D.; Fink, G. *Macromolecules* **1998**, *31*, 4669, 4674, 4681, 4684.
(6) Yoshida, Y.; Saito, J.; Mitani, M.; Takagi, Y.; Matsui, S.; Ishii, S.; Nakano, T.; Kashiwa, N.; Fujita, T. *Chem. Commun.* **2002**, 1298.
(7) Benedikt, G.; Elce, E.; Goodall, B. L.; Kalamarides, H. A.; McIntosh, L. H.; Rhodes, L. F.; Selvy, K. T.; Andes, C.; Oyler, K.; Sen, A. *Macromolecules* **2002**, *35*, 8978.
(8) De Rosa, C.; Corradini, P.; Buono, A.; Auriemma, F.; Grassi, A.; Altamura, P. *Macromolecules* **2003**, *36*, 3789. De Rosa, C.; Buono, A.; Auriemma, F.; Grassi, A. *Macromolecules* **2004**, *37,* 9489.
(9) (a) Natta, G.; Dall'Asta; G.; Mazzanti, G.; Pasquon, I.; Valvassori, A.; Zambelli, A. *J. Am. Chem. Soc.* **1961**, *83*, 3343. (b) Natta, G.; Dall' Asta, G.; Mazzanti, G.; Pasquon, I.; Valvassori, A.; Zambelli, A. *Makromol. Chem.* **1962**, *54*, 95.
(10) (a) Natta, G.; Corradini, P.; Ganis, P.; Bassi, I. W.; Allegra, G. *Chim. Ind.* **1962**, *44*, 532. (b) Natta, G.; Allegra, G.; Bassi, I. W.; Corradini, P.; Ganis, P. *Macromol. Chem.* **1962**, *58*, 242. (c) Corradini, P.; Ganis, P. *Macromol. Chem.* **1963**, *62*, 97.
(11) Arndt, M.; Beulich, I. *Macromol. Chem. Phys.* **1998**, *199*, 1221.
(12) Harrington, B. A.; Crowther, D. J. *J. Mol. Catal. A: Chem.* **1998**, *128*, 79.

(13) Cherdron, H.; Brekner, M.-J.; Osan, F. *Angew. Makromol. Chem.* **1994**, *223*, 121.
(14) Grassi, A.; Maffei, G.; Milione, S.; Jordan, R. F. *Macromol. Chem. Phys.* **2001**, *202*, 1239. Altamura, P.; Grassi, A. *Macromolecules* **2001**, *34*, 9197.
(15) McKnight, A. L.; Waymouth, R. M. *Macromolecules* **1999**, *32*, 2816.
(16) Naga, N.; Imanishi, Y. *Macromol. Chem. Phys.* **2002**, *203*, 159.
(17) Naga, N.; Tsubooka, M.; Suehiro, S.; Imanishi, Y. *Macromolecules* **2002**, *35*, 3041.
(18) Naga, N.; Tsubooka, M.; Sone, S.; Tashiro, K.; Imanishi, Y. *Macromolecules* **2002**, *35*, 9999.
(19) Jerschow, A.; Ernst, E.; Hermann, W.; Müller, N. *Macromolecules* **1995**, *28*, 7095.
(20) Kelly, W. M.; Wang, S.; Collins, S. *Macromolecules* **1997**, *30*, 3151.
(21) Fujita, M.; Coates, G. W. *Macromolecules* **2002**, *35*, 9640.
(22) Lavoie, A. R.; Ho, M. H.; Waymouth, R. M. *Chem. Commun.* **2003**, *104*, 864.
(23) Lavoie, A. R.; Waymouth, R. M. *Tetrahedron* **2004**, *60*, 7147.
(24) Auriemma, F.; De Rosa, C.; Esposito, S.; Coates, G. W.; Fujita, M. *J. Am. Chem. Soc.* **2005**, *127*, 2850.
(25) Wu, Z.; Benedicto, A. D.; Grubbs, R. H.*Macromolecules* **1993**, *26*, 4975.
(26) Cromer, D. T.; Mann, J. B. *Acta Crystallogr.* **1968**, *A24*, 321.
(27) (a) Klug, H. P.; Alexander, L. E. *X-Ray Diffraction Procedures for Polycrystalline and Amorphous Materials*; Wiley-Interscience: New York, 1974. (b) Buerger, M. J. *Crystal Structure Analysis*; John Wiley & Sons: New York, 1960.
(28) *Cerius*^{2} *Modeling Environment*; Molecular Simulations Inc.: San Diego, CA, 1999.
(29) Dinur, U.; Hagler, A. T. New Approaches to Empirical Force Fields. *Rev. Comput. Chem.* **1991**, *2*, 99. Maple, J. R.; Dinur, U.; Hagler, A. T. *Proc. Natl. Acad. Sci. U.S.A.* **1988**, *85*, 5350. Sun, H.; Mumby, S. J.; Maple, J. R.; Hagler, A. T. *J. Am. Chem. Soc.* **1994**, *116*, 2978. Sun, H. *Macromolecules* **1994**, *26*, 5942. Sun, H. *Macromolecules* **1995**, *28*, 701.
(30) IUPAC, Commission on Macromoleculare Nomenclature, *Pure Appl. Chem.* **1981**, *53*, 733.
(31) Corradini, P. In *The Stereochemistry of Macromolecules*; Ketley, A. D., Ed.; Marcel Dekker: New York, 1968; Vol. 3.
(32) Kilpatrick, J. E.; Pitzer, K. S.; Spitzer, R. *J. Am. Chem. Soc.* **1947**, *69*, 2483.
(33) Pitzer, K. S.; Donath, W. E. *J. Am. Chem. Soc.* **1959**, *81*, 3213.
(34) Hendrickson, J. B. *J. Am. Chem. Soc.* **1961**, *83*, 4537; **1963**, *85*, 4059 (erratum).
(35) Lifson, S.; Warshel, A. *J. Chem. Phys.* **1968**, *49*, 5116.
(36) Ferguson, D. M.; Raber, D. J. *J. Am. Chem. Soc.* **1989**, *111*, 4371.
(37) Ferguson, D. M.; Gould, I. R.; Glauser, W. A.; Kollmann, P. A. *J. Comput. Chem.* **1992**, *13*, 535.
(38) Cui, W.; Allinger, N. L. *J. Am. Chem. Soc.* **1993**, *115*, 2943.
(39) Bauman, L. E.; Laane, J. *J. Phys. Chem.* **1988**, *92*, 1040.
(40) Ruiz de Ballesteros, O.; Cavallo, L.; Auriemma, F.; Guerra, G. *Macromolecules* **1995**, *28*, 7355.
(41) Dunitz, J. D. *X-Ray Analysis and Structure of Organic Molecules*; Cornell University Press: Ithaca, NY, 1979.
(42) Auriemma, F.; De Rosa, C.; Corradini, P. *Macromol. Chem. Phys.* **2004**, *205*, 390.
(43) Ruiz de Ballesteros, O.; Venditto, V.; Auriemma, F.; Guerra, G.; Resconi, L.; Waymouth, R. M.; Mogstad, A. *Macromolecules* **1995**, *28*, 2383.
(44) Ruiz de Ballesteros, O.; Cavallo, L.; Auriemma, F.; Guerra, G. *Macromolecules* **1995**, *28*, 7355.
(45) Antinucci, S.; Monaco, G.; Immirzi, A. *Macromolecules* **2001**, *34*, 8078.

MA050659V